Desalination and Water Treatment
www.deswater.com
doi: 10.1080/19443994.2013.810357

52 (2014) 4681–4688
July

Taylor & Francis
Taylor & Francis Group

Effect of some safe additives and mixed salts scales on electrochemical corrosion behavior of yellow brass alloy in artificial seawater

Khadijah M. Emran[a,*], Samia K. Hamdona[b], Abeer Mohammed Al Balawi[a]

[a]*Applied Chemistry Department, College of Applied Science, Taibaj University, P.O. Box (4050), Al-Madinah Al-Monawarah, Kingdom of Saudi Arabia*
Tel./Fax:+ 966 4 8490272; email: kabdalsamad@taibahu.edu.sa
[b]*National Institute of Oceanography and Fisheries, Alexandria, Egypt*

Received 11 August 2012; Accepted 7 May 2013

ABSTRACT

Study of the brass/synthetic seawater interface, with and without inhibitor, was carried out using electrochemical methods. EIS showed that the alloys safer localize corrosion in seawater. The presence of scales decreases the corrosion rate. The inhibition performance of tyrosine (Tyr), polyacrylic acid (PAA), and yeast was studied. The acceleration effect of corrosion processes of brass in the presence of Tyr and PAA reflects that the inhibitor concentration was not enough to completely cover the active surface site of the metal. The protection values of the additives in the case of brass go in the order Tyr > PAA> Yeast.

Keywords: Corrosion; Scales; Safely additives; Brass alloy; Seawater

1. Introduction

Scale formation is especially important in water treatment and thermal desalination plants. Under the effect of temperature, both sea and brackish water show a strong tendency to scale formation, corrosion, and fouling problems, due to the dissolved salts and the finely suspended solids in their solutions [1].

Corrosion in desalination plants can cause a variety of undesirable consequences, including loss of equipment, unplanned shutdowns, expensive repairs, leaks, and contamination of products as well as serious personal hazards [2]. In process industries like desalination plants, corrosion consideration outweighs the other factors while carrying out the material selection for plant constructions [3]. Although the chemistry of sea and brackish waters is complex and there is a large combination of ions that may lead to formation of scale, it is commonly accepted that the four main scale-forming constituents are calcium bicarbonate, calcium sulfates, magnesium salts, and silica [4].

Brass is commercially used as heat exchanger tubes in power plants, desalination plants, oil refineries, and petrochemical plants. Thus, the selection and corrosion control of metals are synonymous as far as safe operation and maximum output from the plant facilities are concerned [5–8]. Historically polymeric, non-polymeric, metals, and amino acids additives have been used in these processes to prevent the formation and deposition of scaling salts [9–12]. The *present work aims* to study the corrosion of brass electrochemically and

*Corresponding author.

scale inhibition by some additives: tyrosine (Tyr), polyacrylic acid (PAA), and yeast. To our knowledge, this is the first time that yeast has been used as inhibitor for corrosion of metals.

2. Experimental

2.1. Specimen and synthetic seawater preparation

Yellow brass plates with dimensions of approximately 100 mm × 200 mm were used as the material for the corrosion and had the composition of (wt) 63% Cu, 34% Zn, and 3% Si, Al. The specimens were polished mechanically to a mirror finish with emery papers. Then, the samples were thoroughly washed with bi-distilled water and then with ethanol (A.R). One face was used; the other face was masked by chemically inert resin.

Artificial seawater was prepared from reagent grade chemicals as recorded in the Table 1. The degree of salinity of this water is 35% [13]. This experiment was carried out using 5 ppm of tyrosine, polyacrylic acid, and yeast added solely to the solution.

2.2. Electrochemical measurements

A three-electrode corrosion cell (volume 0.25 L) was used for the electrochemical measurements. The analytical reagents $CaCl_2$, Na_2SO_4, and Na_2CO_3 were dissolved in double distilled water and filtered through membrane filters (0.22 μm millipore) to produce $CaSO_4{\cdot}2H_2O$ and $CaCO_3$ scales by co-precipitation. For the mixed calcium sulfate and calcium carbonate system, the relative significance of the salts was determined with constant total calcium content (0.09 M).

The electrochemical cell was connected to ACM Gill AC instrument and to a computer. The brass working electrode (WE) was aligned vertically. The experiments were performed under static aerated conditions at l temperature adjusted to 25°C while the electrochemical behavior of Brass in seawater at different temperatures (25–55 °C) was investigated by EIS. A platinum wire and a saturated calomel electrode were used as the counter and reference electrode, respectively.

Table 1
Composition of synthetic seawater [salinity 35%]

Composition	NaCl	Na_2SO_4	KCl	$CaCl_2$	$MgCl_2$
Mol l^{-1}	0.4266	0.0293	0.0106	0.0108	0.0552
g/Kg solution	24.061	4.011	0.761	1.153	5.069

After immersion of the specimen, prior to the impedance measurement, a stabilization period of 20 min was found, which proved sufficient for E_{ss} (the steady-state potential). The AC frequency rang extended from 30 kHz to 0.1 Hz, a 10 mV peak-to-peak sine wave being the excitation signal. Potentiodynamic polarization curves were obtained with a potential sweep rate of 1 mV/s. The potential was swept from cathodic to anodic directions after impedance run.

3. Results and discussion

3.1. The effect of synthetic seawater and scales on brass

The EIS measurements were carried out for brass in artificial seawater after the alloy reached E_{ss}. The impedance spectra recorded for the examined brass in seawater are shown in Fig. 1(a). For simplicity, we assumed that these curves consist of one depressed capacitive loop, followed by a pseudo-inductive loop at end (low frequencies). Goncalves et al. [14] revealed the depressing of capacitive loops to inhomogeneity of the surface structure due to adsorption processes.

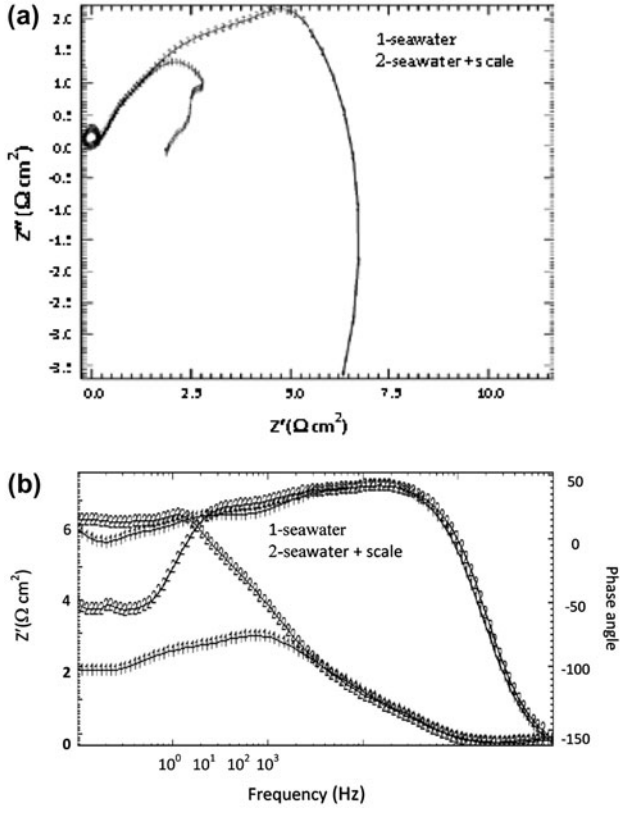

Fig. 1. Impedance plots of Brass in seawater without and with scale: (a) Nyquist plots (b) Bode plots.

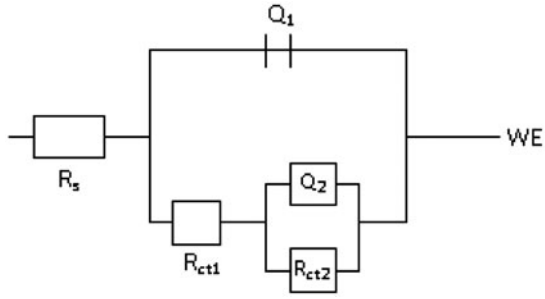

Fig. 2. Equivalent circuit model for the metal suffering localized attack. R_s; solution resistance; R_{ct1}; charge transfer resistance; Q_1; and double-layer capacitance. R_{ct2}: electrolytic resistance through the pit; Q_2; and the pit capacity.

The capacitive loop occurred mainly due to the combination of the charge transfer resistance and the capacitance at the brass/solution interface (dielectric properties of the surface) [15], while the inductive loop at low frequencies indicating localized attack by high [Cl^-]. These observations can be confirmed by corresponding Bode plots in Fig. 1(b) for brass corrosion. In the high frequency (HF) region, Bode plot exhibits constant θ_{max} (phase angle) values vs. frequency (F) with a phase angle lower than 50° which resulted from the phase shift due to the slow potentiostat used for measuring in commercial potentiostats because of the desire for improved stability [16]. This region is responsible for the electronic resistance R_Ω or R_s (resistive region) in Z' ($\Omega\,cm^2$) vs frequency (F) curve. Phase angle spectra present one time constant (one relaxation time) which remains approximately constant over a wide frequency range. Maximum value in the phase angle curve with the phase angle is close to 49°, suggesting that the electrochemical process occurring at HF prevents the formation of the protective film [17]. The constant phase element, CPE, is introduced in the circuit instead of a pure double-layer capacitor in order to take into account the electrode surface heterogeneity resulting from surface roughness, impurities, dislocations, grain boundaries, adsorption of inhibitors, and formation of porous layers [18,19], and therefore to give a more accurate fit [19]. The impedance of the CPE is expressed as:

$$Z_{CPE} = \frac{1}{Q(j\omega)^n} \quad (1)$$

where Q is the magnitude of CPE (in $\Omega^{-1}\,s^n\,cm^{-2}$), ω is the sine wave modulation angular frequency (in rad s^{-1}), $j^2 = -1$ is the imaginary number, and n is an empirical exponent ($0 \leqslant n \leqslant 1$) which measures the deviation from the ideal capacitive behavior [20,21].

Analysis of the impedance spectra was done by fitting the experimental data to the equivalent circuit (EC). The quality of fitting to the EC was judged firstly by the Chi-square ($\chi^2 = 10^{-2}$–10^{-3}) values and, secondly, by the error distribution vs. frequency, comparing experimental results with simulated data.

The Nyqusit diagrams in seawater which consist of inductive part at low frequencies were fitted to the EC shown in Fig. 2. The low frequency (LF) loop corresponds to a localized attack process and the HF loop to a charge transfer behavior. This EC confirms that the lower impedance estimated from the alloy surface was attributed to the distribution of the current between the pit sites and general corrosion spaces [22]. Corrosion kinetic parameters derived from EIS measurements are given in Table 2.

Electrochemical result of brass in the presence of scale is shown in Fig. 1. Increases of the diameter of a capacitive arc with a lower end of the loop crossing the real axis were found. The capacitive arc (first relaxation time in bode plot, Fig. 1(b)) is related with the dielectric properties of the formed film on the brass surface at the open circuit potential, but it may also be related with the electric double-layer capacitance at the electrode/solution interface, which includes a metal/scale interface followed by a scale/solution interface. The total capacitance loop is related

Table 2
Electrochemical kinetic parameters and corrosion rate obtained by electrochemical methods technique for brass in seawater at 25°C in absence and presence of scales and additives

Impedance				Polarization			
Media	R_{ct} ($\Omega\,cm^2$)	n	IE.R_{ct} (%)	$I_{corr.}$ (mA/cm^2)	E_{pass} (mV/SCE)	I_{pass} (mA/cm^2)	IE.$I_{corr.}$ (%)
Seawater	3.578	0.89	–	7.836	54	6.69	–
Seawater + scale	6.317	0.78	43.36	4.033	−4	4.60	48.53
Yeast	8.485	0.71	57.83	3.133	−35	5.11	55.27
PAA	2.598	0.78	−37.72	10.54	27	6.09	−34.51
Tyr	2.211	0.99	−61.83	12.76	100	4.41	−61.56

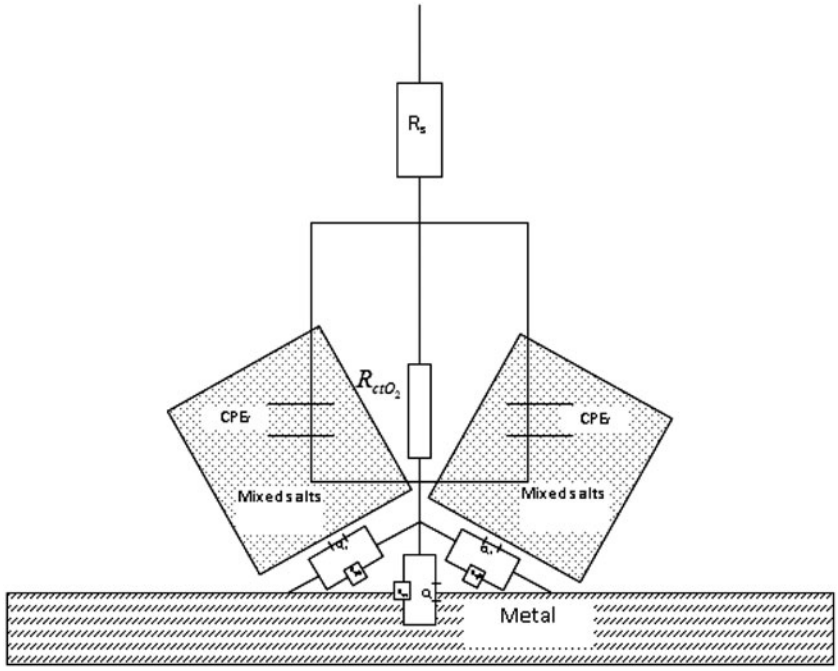

Fig. 3. Equivalent circuit of the impedance diagrams in Fig. 1 and in the presence of scales. Rs is the solution resistance; R_{ctO2} is the charge transfer resistances of oxygen; CPEf is the constant phase element of scale film, R_{ct}: charge transfer resistance; Q; double layer capacity, R_p: electrolytic resistance through the pores, Q_1; and the pit capacity, R_{pit}: electrolytic resistance through the pit.

to the polarization resistance of the scale film, and the second time constant may be attributed to the contribution of oxygen reduction occurring through the porous scale in cavities under the scale crystals by the charge transfer resistance R_{ctO_2}. The low-frequency inductance loop may correspond to localized corrosion through the defects in the scale. The physical model can be illustrated by the EC in Fig. 3 where R_s (Ω cm^2) is the electrolyte resistance; and R_{ctO_2} (Ω cm^2) is the impedance of the scale deposit associated with the finite conductivity of the electrolyte solution in the thin pores in parallel to a capacitance CPE_f (μF/cm^2) related to the dielectric nature of the scale layer. A combination of a capacitive and a pseudo-inductive loop at the LF can be explained by competitive behavior between acceleration and deceleration accompanied with diffusion process on the brass surface [18,23].

The corrosion inhibition percentage efficiencies (IE.%) of the corrosion rate $(R_{ct})^{-1}$ and $(R_{ct(inh.)})^{-1}$ in seawater and in the presence of scale are calculated as follows:

$$\text{IE } \% = \frac{(R_{ct})^{-1} - (R_{ct(inh.)})^{-1}}{(R_{ct})^{-1}} \times 100 \quad (2)$$

$$\text{IEI}_{corr.} \ \% = \frac{i_{corr.} - i_{corr.(inh.)}}{i_{corr.}} \times 100 \quad (3)$$

where R_{ct}, $i_{corr.}$ and $R_{ct(inh.)}$, $i_{corr.(inh.)}$ are the values of charge transfer resistance and corrosion current densities without and with scale, respectively. The impedance derived from these investigations is given in Table 2. A higher polarization resistance (R_{ct} = 6.317 Ω cm^2) compared to the value of the sample in free seawater (R_{ct} = 3.578 Ω cm^2) typically corresponds with a lower corrosion rate. The value of (IE.%) calculated from Eq. (2) is about 43.36%. Martini et al. [24] revealed that for $0.5 < n < 1$, the CPE describes a frequency dispersion of time constants due to local inhomogeneities in the dielectric material surface. The values of n obtained ($\sim$0.78) in Table 2 indicate that the CPE is little associated with the film capacitance processes, where the low value of Q in the presence of scale reflects a protective layer formed on the brass in this condition.

The reaction of copper dissolution (anodic process) is:

$$Cu \rightarrow Cu^+ + \bar{e} \quad (4)$$

Two cathodic processes can be suggested in this case [25]:

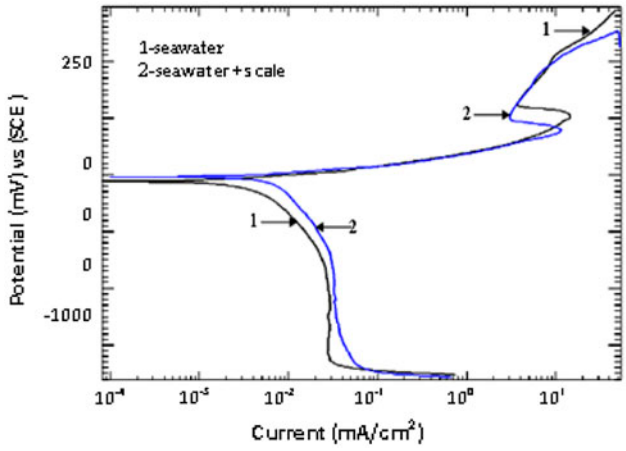

Fig. 4. Potentiodynamic polarization curves of Brass in seawater without and with scale.

- Reduction of the dissolved oxygen (I_{O_2}),

$$O_2 + 2e + 2H_2O \Leftrightarrow H_2O_2 + 2OH^- \quad (5)$$

$$H_2O_2 + 2e \rightarrow 2OH^- \quad (6)$$

- Reduction of water (I_{H_2O}),

$$2H_2O + 2e \Leftrightarrow H_2 + 2OH^- \quad (7)$$

The total cathodic current (I_{total}),

$$I_{total} = I_{O_2} + I_{H_2O} \quad (8)$$

The potentiodynamic polarization curves of brass in seawater in the absence and presence of scale are shown in Fig. 4. The rate of the corrosion process is determined by the corrosion current density ($i_{corr.}$) obtained by extrapolating the Tafel lines on the corrosion potential E_{corr} of the WE and is listed in Table 2. The total cathodic polarization curves are shifted towards an increase in cathodic reaction. This may be due to the increase of potential needed to O_2 reduction in the presence of the scale layer. $I_{corr.}$ values go in opposite direction. In anodic branch, the brass exhibits active–passive behavior at potential ($E_{cp} = 10$ and -55 mV SCE) without and with scale in seawater, respectively. Values of degree of passivation, $I_{pass.}$, of the alloy decreased appreciably with the presence of scale as shown in Table 2. Pseudo passivation may be attributed to a competition between adsorption process by scale ($CaCO_3$ or $CaSO_4$) or corrosion products and selective dissolution of brass results in porous scale film (Scheme 1) on the surface.

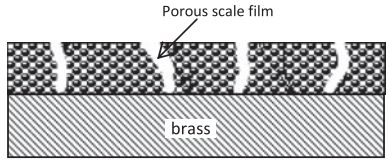

Scheme 1. To investigate that $I_{corr.}$ of Brass in presence scales and seawater has been reduced to 48.53% inspait of in state of the case of sea water only because of incomplete coverage of the surface alloy.

3.2. Effect of additives on the corrosion and electrochemical behavior of brass

An impedance measurement provides information on both the resistive and capacitive behavior at the interface of metal/solution and makes it possible to evaluate the performance of the tested compounds as possible inhibitors against metal corrosion.

In order to evaluate the scale and corrosion inhibition efficiency, three various additives (yeast, PAA, and Try (5 ppm)) were added to seawater with scale (chief 250 ml).

Nyquist plots of brass in seawater solution containing scale and different additives (Fig. 5) consist of two loops. The pseudo-inductive loop at very low frequencies exists in all additive spectra. Two relaxation times were observed in the corresponding Bode-phase plots and the maximum phase angle (θ_{max}) is about 50°. The lowest frequency time constant changes from capacitive to inductive. The pseudo-inductive behavior demonstrates that charge transfer and adsorption reaction occurred.

The experimentally determined impedance parameters corresponding to the impedance measurements, fitted to the suitable EC, are collected in Table 2. These results indicated that the change in the capacity is related to the dielectric nature of the scale formed. Higher values of n obtained in the Tyr solution (0.99 near unity) indicated that the dissolution reaction is under charge transfer control. The increase in the capacity of the scale layer in the presence of PAA and Try reflects the increase in the porosity of the scale film. The aggressive ions diffuse through this layer and reach the brass at the brass/scale interface.

Negative values of IE.R_{ct}% indicate the acceleration effect of additives. It is commonly assumed that the corrosion inhibition of surfactant molecules is directly proportional to the surfactant's coverage on the surface of metal. When the concentration of the inhibitor

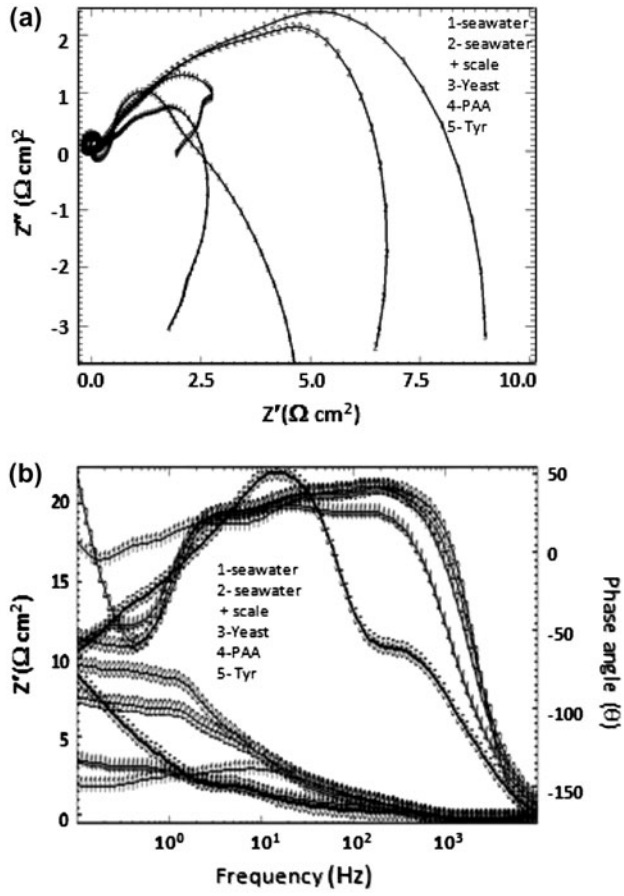

Fig. 5. Impedance plots of Brass in seawater in the presence of different additives: (a) Nyquist plots (b) Bode plots.

is not enough to completely cover the active surface sites of the metal, the inhibitor will accelerate the corrosion processes.

The potentiodynamic polarization curves of brass in seawater, seawater scale, and seawater scale within the additives (yeast –PAA—Tyr) are shown in Fig. 6. The cathodic polarization curves are shifted towards an increase in reduction reaction. Kinetic parameters calculated from the polarization curve are listed in Table 2. The lower values of both $I_{corr.}$ and I_{pass} reflect the best protection of brass surface by yeast which agrees with impedance data. The presence of PAA or Tyr decreases the brass resistivity (high value of $I_{corr.}$ and negative values of IE.$I_{corr.}$). From curves in Fig. 6, it can be observed that active–passive transition occurs at a more positive potential, and the potential needed to reach the passivity region increases ($E_{corr.}$–E_{pass} = 305 and 400 mV (SCE) respectively), which means that the presence of PAA or Tyr markedly delayed the protection process. The protective action of the additive is clearly observed by R_{ct} and IE.R_{ct}% values in the Table 2, which gives the following order: Tyr > PAA > Yeast.

3.3. Temperature effect on Brass corrosion

Temperature can modify the interaction between the metal and the electrolyte. It is well known that temperature has a great effect on the electrochemical behavior, the corrosion rate of metals, and the scale precipitation on it.

The electrochemical behavior of brass in seawater at different temperatures was investigated by EIS. EIS spectra obtained in artificial seawater at temperature range 25–55˚C (Fig. 7(a)) consist of a capacitive arc with a pseudo-inductive loop regardless of the solution temperature. The first time constant observed corresponding to the brass/electrolyte interface revealed a charge transfer control for the system. The pseudo-inductive loop reflects the competitive process between the local attack and scale precipitation.

Acceptable converge between the experimental and fitted data was found. The values of the parameters determined at various temperatures on the basis of the structure model offered are summarized in Table 3.

Most probably, the acceleration of the anodic process occurs quicker at higher temperatures, and this reflects the inductive loop at the end of the Nyquist plot and decrease in brass resistivity, which indicates that the Faradic process takes place on the brass surface free of protective film. Values of corrosion rate mm/y also increase and reach unacceptable values [26]. The corrosion rate at 55˚C increases about 3.44 times from 25˚C. If n is accepted to be the measure of

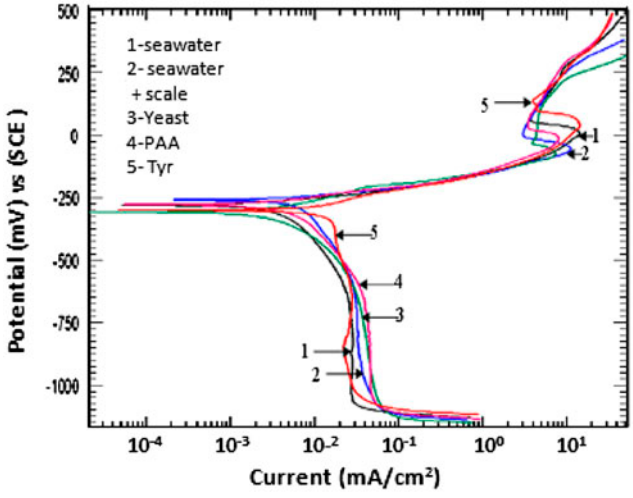

Fig. 6. Potentiodynamic polarization curves of Brass in seawater in the presence of different additives.

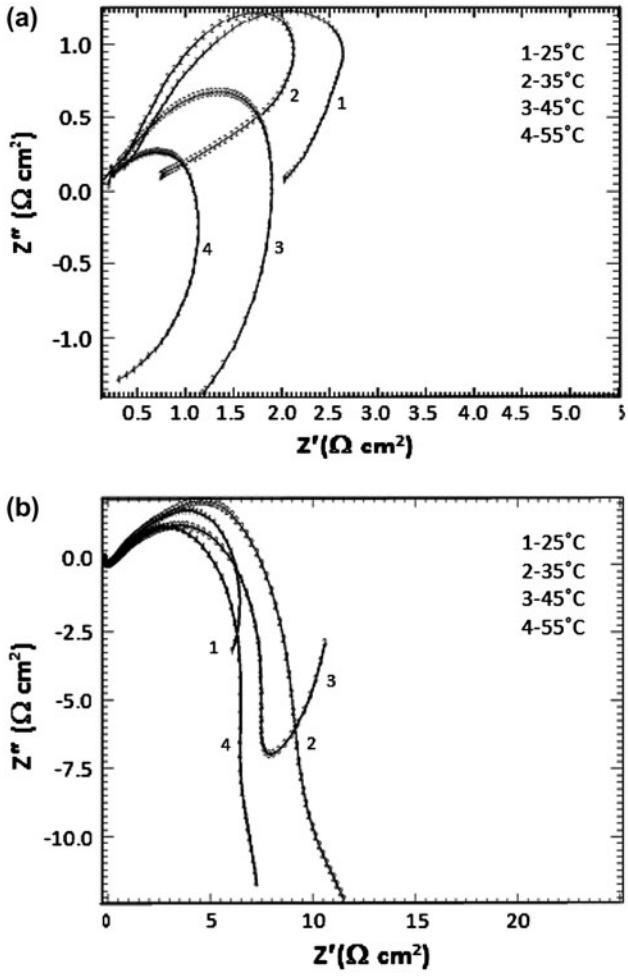

Fig. 7. Impedance plots of Brass at different temperatures in seawater: (a) without, (b) with scale.

the surface inhomogeneity, then its decrease should be connected with a certain increase in heterogeneity resulting from surface alloy roughening. The latter may be caused by enhanced dissolution of alloy, which takes place at high temperatures during exposure to the solution. This effect is accompanied by an increase in the corroded area (increase in Q values). The low values of n in seawater at a range of 25–55°C may be connected with two effects: a certain drawing of the formation/distortion equilibrium towards distortion and roughening of the alloy surface which resulted from enhanced corrosion.

In the presence of scale, impedance spectra at HF exhibit a single capacitive loop (one relaxation time) at different temperatures as shown in Fig. 7(b). In spite of scale presence, brass is less resistive to localized corrosion with the temperature increase. Higher values of R_{ct} in the presence of scale indicate that the scale is formed at high temperature but does not completely cover the metal surface. The bare brass surface quickly corroded as temperature rose. The decrease in R_{ct} values is associated with the increase in Q values as shown in Table 3. This was confirmed both by the presence of pseudo-inductive loop and the large value of corrosion rate mm/y in Table 3.

Table 3
Electrochemical kinetic parameters and corrosion rate obtained by EIS technique for brass in seawater at different temperatures

t (°C)	Without scales			With scales		
	R_{ct} ($\Omega\,cm^2$)	n	Corrosion rate (mm/y)	R_{ct} ($\Omega\,cm^2$)	n	Corrosion rate (mm/y)
25	3.578	0.89	147.6	6.317	0.78	83.63
35	2.971	0.74	170.4	7.181	0.77	73.56
45	1.819	0.69	290.4	6.206	0.68	85.12
55	1.039	0.65	508.1	5.129	0.69	101.5

The diagram at 35°C shows a capacitive arc with a higher R_{ct} value at high frequencies range followed by a tail at lower frequencies. The tail is probably associated with the mass transport process in the solution. This is due to the formation of a porous layer of scale on the brass surface. The low values of n indicate that slightly low homogeneity of the surface may be due to the computation between both the corrosion and the scale formation on the surface.

4. Conclusion

The present study demonstrates the corrosion and electrochemical behavior of brass in the absence and presence of scales and the development of inhibitors for the cooling system. By analyzing electrochemical data, the main finding are:

(1) Brass suffers pitting corrosion in the artificial seawater.
(2) The presence of scale decreases the corrosion rate.
(3) Corrosion tests in the presence of yeast showed remarkable protection against corrosion and scale formation.
(4) In the presence of the additives, the protection values of the additives for Brass alloy goes in order: Tyr > PAA > Yeast.
(5) Acceleration of anodic process occurs quicker at higher temperatures and this reflects the inductive loop at the end of the Nyquist plot. In spite of the scale presence, brass is less resistive to localized corrosion with the temperature increase.

References

[1] J.G. Knudsen, Fouling in heat exchangers, in: G.F. Hewitt (Ed.), Hemisphere Handbook of Heat Exchangers Design, Hemisphere, New York, NY, 1990.

[2] H.G. Heitmann, Saline Water Processing, VCH, Weinheim, 1990.

[3] J.W. Oldfield, B. Todd, Vapour side corrosion in MSF plants, Desalination 66 (1987) 171–184.

[4] X. Ouyang, X. Qiu, H. Lou, D. Yang, Corrosion and scale inhibition properties of sodium lignosulfonate and its potential application in recirculating cooling water system, Ind. Eng. Chem. Res. 45(16) (2006) 5716–5721.

[5] H. Gerengi, K. Darowicki, G. Bereket, P. Slepski, Evaluation of corrosion inhibition of brass-118 in artificial seawater by benzotriazole using Dynamic EIS, Corros. Sci. 51 (2009) 2573–2579.

[6] A.R. Rakitin, V.I. Kichigin, Electrochemical study of calcium carbonate deposition on iron. Effect of the anion, Electrochim. Acta 54 (2009) 2647–2654.

[7] S. Muryanto, A.P. Bayuseno, W. Sediono and W. Mangestiyono, Education for chemical engineers "Development of a versatile laboratory project for scale formation and control," Educ. for Chem. Eng. 7(3) (2012) 78–84.

[8] E.I. Shaheen, S.N.S. Dixit, Scale reduction in saline water conversion, Desalination 13 (1973) 187–206.

[9] S.K. Hamdona, R.B. Nessim, S.M. Hamza, Spontaneous precipitation of calcium sulphate dihydrate in the presence of some metal ions, Desalination 94 (1993) 69–80.

[10] J.S. Gill, A novel inhibitor for scale control in water desalination, Desalination 124 (1999) 43–50.

[11] S.K. Hamdona, O.A. Al Hadad, Influence of additives on the precipitation of gypsum in sodium chloride solutions, Desalination 228 (2008) 277–286.

[12] M. Finsgar, S. Fassbender, S. Hirth, I. Milosev, Electrochemical and XPS study of polyethyleneimines of different molecular sizes as corrosion inhibitors for AISI 430 stainless steel in near-neutral chloride media, Mat. Chem. Phys. 116 (2009) 198–206.

[13] K.H. Khoo, R.W. Ramette, C.H. Culberson, R.G. Bates, Determination of hydrogen ion concentrations in seawater from 5 to 40°C: Standard potentials at salinities from 20 to 45‰, Anal. Chem. 49 (1997) 29–34.

[14] R. Simões Gonçalves, D. Schermann Azambuja, A.M. Serpa Lucho, Electrochemical studies of propargyl alcohol as corrosion inhibitor for nickel, copper, and copper/nickel (55/45) alloy, Corros. Sci. 44 (2002) 467–479.

[15] I. Bentova, M. Bojinov, T. Tzvetkoff, Oxidative dissolution and anion-assisted solubilisation in the transpassive state of nickel–chromium alloys, Electrochim. Acta 49 (2004) 2295–2306.

[16] F.B. Mansfeld, W.M. Kendig, S. Tsai, Recording and analysis of alternating current impedance data for corrosion studies; Part 2—Experimental approach and results, Corrosion 38 (1982) 570–580.

[17] P. Girault, J.L. Grosseau-Poussard, J.F. Dinhut, L. Marechal, Influence of a chromium ion implantation on the passive behaviour of nickel in artificial sea-water: An EIS and XPS study, Nucl. Instrum. Methods Phys. Res., Sect. B, 174 (2001) 439–452.

[18] S.T. Arab, K.M. Emran, Influence of cr addition on the electrochemical behavior of Ni–base metallic glasses in HCl, Phys. Chem. News 50 (2009) 130–138.

[19] A.U. Malik, S. Ahmad, I. Andijani, S. Al-Fozan, Corrosion behavior of steels in Gulf seawater environment, Desalination 123 (1999) 205–213.

[20] J.R. Macdonald, W.B. Johanson, J.R. Macdonald (Ed.), Theory in Impedance Spectroscopy, John Wiley, New York, 1987.

[21] Z.B. Stoynov, B.M. Grafov, B. Savova-Stoynova, V.V. Elkin, Electrochemical Impedance, Nauka, Moscow, 1991.

[22] S.T. Arab, K.M. Emran, H.A. Al-Turaif. J. Saudi Chem. Soc. (in press). Available from: http://www.sciencedirect.com/science/article/pii/S1319610311001190 (accessed 12 June).

[23] S.T. Arab, K.M. Emran, H.A. Al-Turaif, The electrochemical behavior of Ni-base metallic glasses containing Cr in H_2SO_4 Solutions, J. Korean Chem. Soc. 53(3) (2009) 448–458.

[24] E.M.A. Martini, S.T. Amaral, I.L. Müller, Electrochemical behaviour of Invar in phosphate solutions at pH = 6.0, Corros. Sci. 46 (2004) 2097–2115.

[25] O. Devos, C. Gabrielli, B. Tribollet, Simultaneous EIS and *in situ* microscope observation on a partially blocked electrode application to scale electrodeposition, Electrochim. Acta 51 (2006) 1413–1422.

[26] G. Fontana, Corrosion Engineering, third ed., McGraw Hill International, New York, NY, 1987.